Geoderma 379 (2020) 114636

Contents lists available at ScienceDirect

Geoderma

journal homepage: www.elsevier.com/locate/geoderma

Impact of differences in soil temperature on the desert carbon sink

Fan Yang[a,b], Jianping Huang[a,c,*], Qing He[b], Xinqian Zheng[d], Chenglong Zhou[b], Honglin Pan[b], Wen Huo[b], Haipeng Yu[c], Xiaoyue Liu[a], Lu Meng[b], Dongliang Han[c], Mamtimin Ali[b], Xinghua Yang[b]

[a] College of Atmospheric Sciences, Lanzhou University, Lanzhou, China
[b] Taklimakan Desert Meteorology Field Experiment Station of CMA, Institute of Desert Meteorology, China Meteorological Administration, Urumqi, China
[c] Collaborative Innovation Center for Western Ecological Safety, Lanzhou University, Lanzhou, China
[d] Xinjiang Agro-Meteorological Observatory, Urumqi, China

Keywords:
Taklimakan Desert
Soil respiration
Soil temperature difference
Desert carbon sink
Expansion/contraction
Climate change

ARTICLE INFO

Editor Name: Ingrid Kögel-Knabner.

ABSTRACT

An understanding of the global terrestrial carbon cycle is crucial to predict future climate change. Deserts are an important part of the terrestrial ecosystem, but their role in the terrestrial carbon cycle has long been neglected. Recent studies have shown that deserts may sequester enormous volumes of CO_2 and play a pivotal role as a carbon sink. As the world's second-largest shifting desert, the Taklimakan Desert (TD) contributes substantially to the global desert carbon sink. However, the contributions of the internal processes of the TD to its carbon sink and the long-term trend of the carbon sink under climate change are still unclear. Based on an observational study, we determined that both the expansion/contraction of soil air containing CO_2 caused by heat fluctuation in shifting sand and the salt/alkali chemistry control the release/absorption processes of soil respiration in shifting sand. Besides, the mutual offset of these processes indicates that the shifting sand in the TD acts as a stable carbon sink at present, with an annual average CO_2 uptake rate of 7.11 g m^{-2}. However, an increase in soil temperature difference will stimulate soil air expansion and release more CO_2 into the atmosphere under climate change, gradually lessening the carbon sink rate of shifting sand in TD in the future. These processes will be accelerated by a positive feedback loop, where this effect triggered by climate change will enhance regional warming. Our results highlight the status of deserts in the global carbon cycle and provide crucial information regarding the world's missing carbon sink.

1. Introduction

Soil respiration (soil-to-atmosphere CO_2 flux) is the major route for carbon to enter the atmosphere from soil (Singh and Gupta, 1977; Schlesinger and Andrews, 2000; Lou and Zhou, 2006). The estimated amount of carbon released worldwide from the soil into the atmosphere is 91–94 Pg C annually, with an annual increase of 0.04 Pg C through this process (Xu and Shang, 2016; Bond-Lamberty, 2018; Jian et al., 2018). This process determines the carbon cycle of terrestrial ecosystems to some extent (Hashimoto et al., 2015). Even slight variation in this process can have far-reaching effects on the atmospheric CO_2 concentration and could facilitate a positive feedback effect under climatic change (Houghton et al., 1998; Rustad et al., 2000; Friedlingstein et al., 2001; Li et al., 2018; Han et al., 2018). Generally, soil respiration is the total contribution of biological and abiotic processes in the soil, and is extremely sensitive to environmental change. In ecosystems with relatively high productivity, soil respiration is very strong due to the active biological processes, primarily the respiration of plant roots and soil microorganisms. The contribution of abiotic processes (such as dissolution/diffusion of CO_2, adsorption/desorption of CO_2, dissolution/precipitation of carbonate, UV

* Corresponding author at: College of Atmospheric Sciences, Lanzhou University, Lanzhou, China.
E-mail address: hjp@lzu.edu.cn (J. Huang).

https://doi.org/10.1016/j.geoderma.2020.114636
Received 2 June 2020; Received in revised form 27 July 2020; Accepted 27 July 2020
Available online 09 August 2020

decomposition of organic carbon, and chemical oxidation of carbon-containing compounds in soil) to soil respiration is often low and easy to ignore. However, in an extreme environment with relatively low productivity (such as saline soils, the Gobi, Desert, and polar dry valleys), the contribution of abiotic processes to soil respiration cannot be ignored (Parsons et al., 2004; Shanhun et al., 2012; Chen et al., 2014). The contribution of abiotic processes may even dominate in some extreme environments (Ball et al., 2009). In addition, negative CO_2 fluxes (i.e., CO_2 uptake by the soil) have been noted in several extreme environments, suggesting that these environments may be a CO_2 sink (Stone, 2008; Li et al., 2015).

In the global carbon cycle, about 1.8 Pg carbon is missing every year, i.e., the missing carbon sink, which has puzzled researchers for a long time (Houghton et al., 1998). The desert ecosystem, as a typical widely distributed extreme environment, has received much interest from the scientific community in recent years due to the discovery that it can store large amounts of CO_2 to reduce the missing carbon sink. By quantitatively resolving the contribution of biological and abiotic processes to soil respiration in deserts, several studies have demonstrated that soil respiration is mainly controlled by abiotic processes (Xie et al., 2009; Wang et al., 2013; Ma et al., 2013, 2014; Fa et al., 2016). Surface turbulence, air volume expansion, exudation of the CO_2 dissolved in soil water, desorption, carbonate precipitation, and decomposition of soil organic matter are the primary CO_2 emissions processes in desert ecosystems (Parsons et al., 2004; Wang et al., 2013; Fa et al., 2016). At the same time, potential chemical reactions may occur in desert saline and alkaline soils under the influence of soil moisture, resulting in carbonate dissolution and the promotion of CO_2 absorption by the soil (Stone et al., 2008; Xie et al., 2009). A reduction in soil temperature (Parsons et al., 2004; Ball et al., 2009; Hamerlynck et al., 2013) and increase in soil moisture (Cuezva et al., 2011; Fa et al., 2014) can rapidly accelerate CO_2 absorption by the soil. In addition, saline-alkali soil with a high pH in deserts can promote CO_2 absorption in lower temperatures (Wang et al., 2013). Similarly, Ma et al. (2013) and Ma et al. (2014)) found that the inorganic CO_2 flux under the control of soil temperature dominated soil respiration in deserts, and soil pH influenced the changes in soil respiration to a certain extent. The inorganic CO_2 flux in the soil at night has been found to be the main cause of carbon sequestration in deserts. In sum, the main abiotic soil carbon sequestration processes are variation in the volume of gases caused by changes in pressure and temperature governed by the ideal gas law; changes in the solubility of CO_2 in soil–water films governed by Henry's Law; pH-mediated CO_2 dissolution chemistry; and surface adhesion of CO_2 onto soil minerals (Parsons et al., 2004; Xie et al., 2009; Fa et al., 2016; Schlesinger, 2017). However, the exact contribution of these abiotic processes to the desert carbon sink and our understanding of their internal combinations and mechanisms are still uncertain. This important knowledge gap prevents us from accurately positioning the status of the desert ecosystem in the carbon cycle, and it is difficult to understand the long-term trend of the desert carbon sink under climate change.

The Taklimakan Desert (TD) is the world's second-largest shifting desert, and has the characteristics of being far from the sea, with a dry climate, sparse vegetation, complex dune types, strong mobility of dunes, large areas of shifting sand, a thick shifting sand layer, and small sand particle size. It is a typical representative of the world's deserts. In this study, the TD was used as a case study to quantitatively evaluate the contribution of each internal soil respiration process within the shifting sand layer to the desert carbon sink and its main driving mechanism through field measurements and laboratory experiments. On this basis, combined with historical environmental monitoring data and Fifth Coupled Model Intercomparison Project (CMIP5) simulations, the long-term trend of the carbon sink rate of shifting sand in TD under climate change was explored. It is very necessary for us to re-recognize the status of deserts in the global carbon cycle and to narrow the gap of the missing carbon sink. The remainder of this paper is organized as follows. Section 2 describes the Materials and Methods, Sections 3 and 4 present the results and discussion, respectively, and Section 5 lists the main conclusions of this study.

2. Materials and Methods

2.1. Site description

The surface of the TD is mainly covered by a homogeneous shifting sand layer. The environmental conditions at the three monitoring sites from north to south were consistent, particularly regarding soil temperature (Fig. 1). Tazhong, located in the hinterland of the desert, was considered the research area most representative of the TD. This study was conducted in the Tazhong shifting sand (38° 58′ N, 83° 39′ E, 1099 m above sea level). The entire region has a continental, warm temperate, arid desert climate. The annual mean precipitation is 25.9 mm, and the intra-annual distribution is exceedingly non-uniform, with precipitation concentrated in May–August. The annual potential evaporation is 3812.3 mm. The region has four distinct seasons and a high diurnal temperature range. The mean annual temperature is 12.1 °C, with maximum temperatures of 40.0–46.0 °C and minimum temperatures of −20.0 to −32.6 °C (Yang et al., 2017; Zhou et al., 2019). Poor environmental conditions have resulted in a severe deficiency in animal- and plant-based resources in this region. The total area of shifting sand in the TD is approximately 2.364×10^{11} m^2, covering around 70% of the TD (Wang et al., 2005). The shifting sand consists of silt and clay (1.5%), fine and very fine sand (88.8%) grains, and medium sand (9.7%) grains. The average particle size of the sand is 0.083–0.129 mm, with a standard deviation between 0.03 and 0.98 mm. Surface sand in this region is finer than that in other deserts (Huo et al., 2011; Yang et al., 2016a). Table 1 displays the physicochemical traits of the shifting sand. The region experiences prevailing easterly winds throughout the year, with an annual mean of 11 days of gale-force weather, more than 157 days with floating dust and blowing sand, and an annual mean of 16 days with sandstorms (Yang et al., 2016b). The aeolian landforms mainly consist of linear, high, and composite longitudinal dunes and inter-dune corridors. The dunes have an NNE–SSW or NE–SW orientation, and their relative height is 40–50 m.

2.2. Disassembly experiment

To facilitate analyses of the contributions of the various components of TD shifting sand to soil respiration and to account for the fact that shifting sand has a simple structure, we hypothesized that soil respiration in shifting sand (R_s) was the sum of the contributions from sand (R_{sand}), moisture ($R_{moisture}$), salt/alkali ($R_{salt/alkali}$), and microbes ($R_{microbe}$) (Eq. (1)). The four processes involved in the soil respiration of the shifting sand fully agree with the current consensus (Parsons et al., 2004; Fa et al., 2014, 2016). The complex interactions between the various components and changes in the carbon storage capacity of each process will be considered in future studies.

$$R_s = R_{sand} + R_{moisture} + R_{salt/alkali} + R_{microbe} \quad (1)$$

We collected topsoil (0–10 cm) from the shifting sand layer at the study site and divided it into four parts (Table 2). Sample 1 was the control and was not treated. Sample 2 was autoclaved to remove the contribution of soil microorganisms to soil respiration. To ensure that sterilization was sufficient, autoclaving was repeated three times, each time for half an hour. The sterilized shifting sand was immediately placed in an oven and dried at 105 °C. The dried shifting sand was sealed tightly before being placed in a sterile UV chamber. Finally, after allowing the sample to stand in a sterile state for one day, a watering can was used to add 17.18 mL distilled water to match the soil water content measured in the field (0.0013 kg kg^{-1}). The shifting sand sample was evenly mixed while the distilled water was added and then

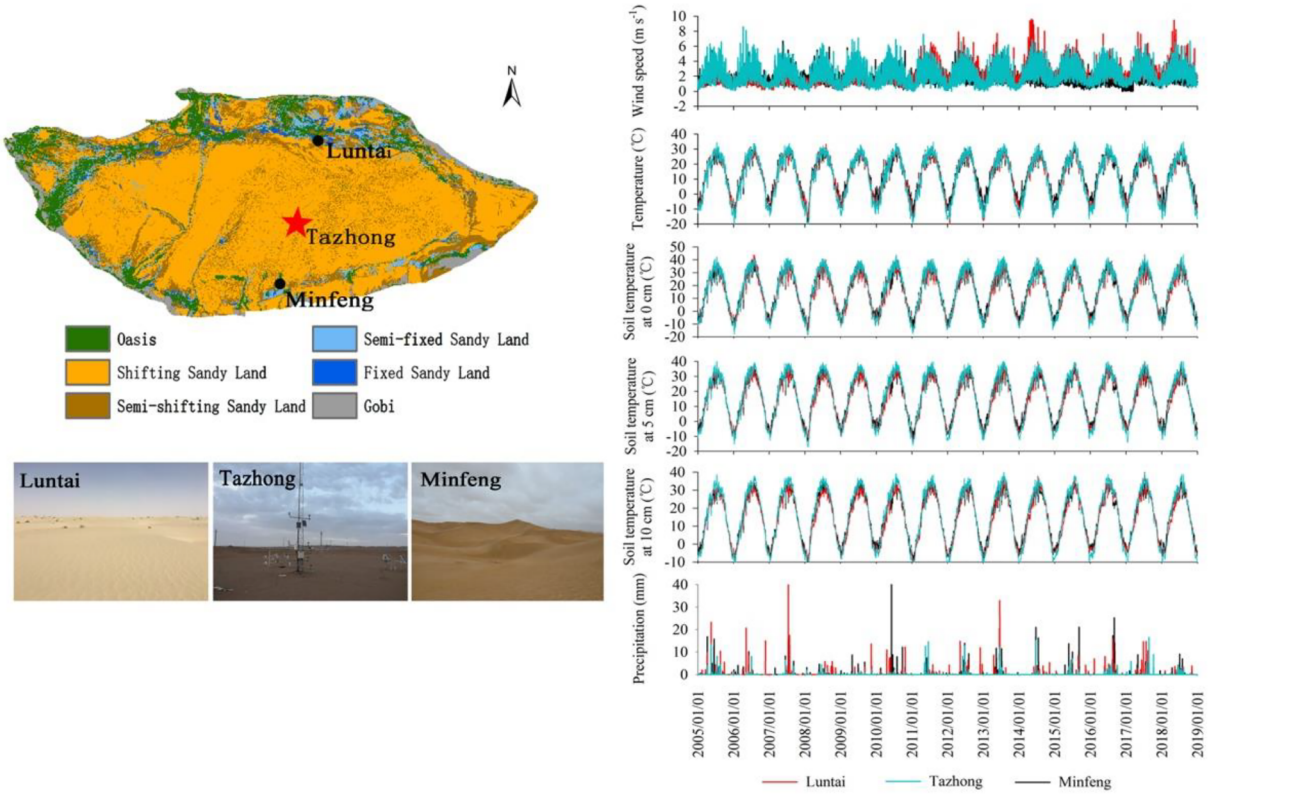

Fig. 1. Left: Distribution of land cover types in the Taklimakan Desert (TD) and the geographical location of Tazhong (red star). Landscape photographs of different locations in the TD, showing that the surface is mainly covered by a wide range of highly homogeneous shifting sand. Right: Comparison of the environmental conditions of the three monitoring points (Luntai, Tazhong, and Minfeng) from north to south in the TD. (For interpretation of the references to colour in this figure legend, the reader is referred to the web version of this article.)

Table 1
Description of the physical and chemical properties of the topsoil of the shifting sand in the hinterland of the Taklimakan Desert (TD) (mean ± standard deviation).

Variable	Depth (cm)	
	0–5	5–10
Average gravimetric soil moisture content (%, kg kg^{-1})	0.0013 ± 0.0002	
Soil total salt (g kg^{-1})	3.45 ± 0.35	9.64 ± 1.10
Soil organic carbon (g kg^{-1})	0.56 ± 0.12	0.63 ± 0.03
Soil total nitrogen (g kg^{-1})	0.06 ± 0.01	0.09 ± 0.02
Ratio of soil organic carbon to soil total nitrogen	9.85 ± 0.83	7.66 ± 1.58
pH	7.33 ± 0.02	7.3 ± 0.04
Bacteria (organisms g^{-1} dry soil)	26,000	4400
Fungi (organisms g^{-1} dry soil)	< 100	< 100
Actinomyces (organisms g^{-1} dry soil) Gu et al. (2000)	238	

was sealed and allowed to stand for two days, so that CO_2 and water in the sample could achieve equilibrium. Sample 3 was placed in plastic boxes and 30 L of distilled water was added to the samples. After being fully mixed, the samples were allowed to stand for 1 h, and then the upper liquid layer was decanted. This procedure was repeated three times to remove soluble salts and alkalis in the sample. Then the treatment method used for sample 2 (three rounds of sterilization, followed by drying, adding distilled water (15.9 mL), and being left to stand) was applied. Sample 4 was subjected to a similar treatment process to that of sample 3, but distilled water was not added.

As shown in Fig. 2, the four samples that were allowed to stand and equilibrate were placed in plastic trays (diameter 40 cm, height 18 cm). One day before soil respiration measurements were taken, the four samples and their plastic trays were buried in the shifting sand, 20 m from the 3 m high land–atmosphere interaction observation tower. The levels of shifting sand inside and outside the tray were kept the same. Four cylindrical soil collars (cross-sectional area of 371.8 cm^2 and a height of 10 cm) were embedded in the four samples up to a depth of 8 cm. From October 10 to 18, 2017, an automatic soil respiration measurement system (model LI-8100A fitted with an LI-8150 multiplexer, LI-COR, Lincoln, NE, USA), equipped with four LI-8100–104 long-term monitoring chambers, was used for whole-day continuous and synchronous monitoring of daily soil respiration dynamics in the four samples. Because soil respiration is weak in deserts, we calibrated the analyzer before obtaining the measurements to ensure precision and appropriately extended the duration of the entire measurement process.

Table 2
Methods of topsoil sample pretreatment.

Sample No.	Contribution of each component	Sample weight (kg)	Pretreatment
1	R_s	13.21	No treatment (control check)
2	R_{sand} + R_{water} + $R_{salt\ /alkali}$	13.22	Autoclaving → Drying → Add distilled water
3	R_{sand} + R_{water}	12.23	Remove soluble salts and alkalis → Autoclaving → Drying → Add distilled water
4	R_{sand}	12.33	Remove soluble salts and alkalis → Autoclaving → Drying

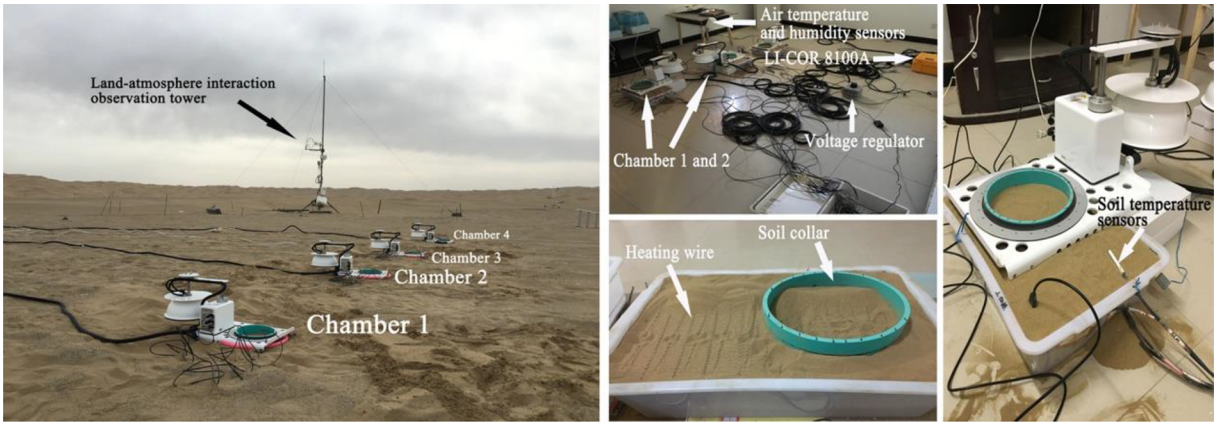

Fig. 2. Layout of the soil respiration experiment. Left: Field monitoring of the contributions of various shifting sand components to soil respiration. Chambers 1–4 correspond to samples 1–4, respectively. The land–atmosphere interaction observation tower provided the historical soil temperature observation data used in this study. Right: Temperature-controlled experimental setup to measure CO_2 flux in sand. Heating wires were placed at a spacing of 2 cm along the surface of the sand in one of the plastic boxes. Soil collars were embedded in the sand. Soil temperature sensors were installed in the sand at depths of 0 and 10 cm.

Further details of the instrument settings during field measurements can be found in Yang et al. (2017). During the experimental period, the seal ring of the chamber was cleaned three times a day to ensure that the chamber was airtight. In addition, to increase our confidence in the application of the LI-8100A instrument to a desert environment, we conducted evaluation experiments in the study area. The bottoms of the soil collars were completely sealed with plastic film and buried in the shifting sand. The plastic film blocked CO_2 exchange between the shifting sand and atmosphere. The respiratory rate of the four chambers did not change with changes in the external conditions, and values were all concentrated near zero, with an accuracy of ± 0.02 $\mu mol \cdot m^{-2} \cdot s^{-1}$. Therefore, the soil respiration of shifting sand obtained by the LI-8100A in this study was considered reliable and accurate. Finally, using step-by-step dismantling, we obtained CO_2 flux data for various components in the TD shifting sand.

2.3. Temperature-controlled experiment

A temperature-controlled experiment was conducted in the basement of the TD meteorological field experiment station to avoid complex and uncontrollable environmental conditions in the field (Fig. 2). During the experimental period, the air temperature in the basement was maintained at approximately 10 °C. The variation in air temperature during the experiment did not exceed 0.79 °C. The mean relative air humidity was 18.32%, and the variation did not exceed 2.9%. The CO_2 concentration was maintained at approximately 405.8 ppm.

Based on the treatment method for sample 4, sand samples were packed into two plastic boxes (length 60 cm, width 45 cm, and height 20 cm). Soil collars were embedded in the boxes. A heating wire was evenly placed, with a spacing of 2 cm, along the surface of the sand in one of the plastic boxes. The temperature of the sand was controlled by adjusting the voltage of the heating wire (Fig. 2). The second box was used as a control and was not heated. From November 21–25, 2017, an automatic soil respiration measurement system was used for synchronous and continuous monitoring of soil respiration in the sand after these two heating treatments. Device settings were identical to those used in the field monitoring experiment. Soil temperature sensors (Model 109, Campbell Scientific, Logan, UT, USA) were installed at depths of 0 and 10 cm in the sand in the two plastic boxes to obtain the soil temperature at the corresponding depths (T_{0cm} and T_{10cm}).

2.4. Statistical analyses

The SPSS 16.0 software was used for the differential analyses of soil respiration in the different treatments. SigmaPlot 14.0 was used for correlation and regression analyses of the soil respiration, the soil temperature difference between 0 and 10 cm ($T_{0–10cm}$, °C), and the rate of soil temperature change at 10 cm ($\Delta T_{10cm}/\Delta t$, $°C \cdot min^{-1}$; soil temperature difference at 10 cm every minute between two consecutive CO_2 flux measurements). Four common nonlinear equations were used to analyze the synergistic effects of $T_{0–10cm}$ and $\Delta T_{10cm}/\Delta t$ on soil respiration:

$$R = a + b\ T_{0-10cm} + c\ (\Delta T_{10cm}/\Delta t) \quad (2)$$

$$R = a + b\ T_{0-10cm} + c\ (\Delta T_{10cm}/\Delta t) + d\ T_{0-10cm}(\Delta T_{10cm}/\Delta t) \quad (3)$$

$$R = a + b\ T_{0-10cm} + c\ (\Delta T_{10cm}/\Delta t) + d\ (T_{0-10cm})^2 + e\ (\Delta T_{10cm}/\Delta t)^2 \quad (4)$$

$$R = a\ T^{b}_{0-10cm}(\Delta T_{10cm}/\Delta t)^c \quad (5)$$

where R is soil respiration (such as R_{sand} or R_s), and a, b, c, d, and e are fitting parameters.

2.5. Estimation of historical soil respiration in TD shifting sand

Based on the regression equations above, we selected the best fitting equation for R_{sand} or R_s, and in combination with the soil temperature observations in the study area at 0 and 10 cm every hour between 2004 and 2017, we estimated the corresponding soil respiration.

2.6. Future trends in soil respiration in TD shifting sand

We would like to use the relationship between soil temperature ($T_{0–10cm}$ and$\Delta T_{10cm}/\Delta t$) and soil respiration in combination with average soil temperature prediction data from multiple models in CMIP5 to expand the timescale across which the relationship was assessed and estimate future soil respiration in the TD shifting sand. However, several problems had to be overcome. Eight models were selected from CMIP5 that simulated data for monthly mean soil temperatures from 2006 to 2100. The simulated surface temperature data were separately verified using monthly mean surface temperature data measured in 2006–2017 in the study area. The three models with the best simulation results were identified. These three models had different soil depth levels and did not directly provide soil temperature at a depth of 10 cm. Using the regression relationship between the observed monthly mean soil temperatures at depths of 0 and 10 cm in the study area from 2006 to 2017, combined with the average surface temperatures of the three selected models, soil temperature at a depth of 10 cm was calculated. The monthly average $T_{0–10cm}$ was obtained from 2017 to 2100. The $\Delta T_{10cm}/\Delta t$ parameter does not retain its original physical meaning on a monthly time scale, so the previously

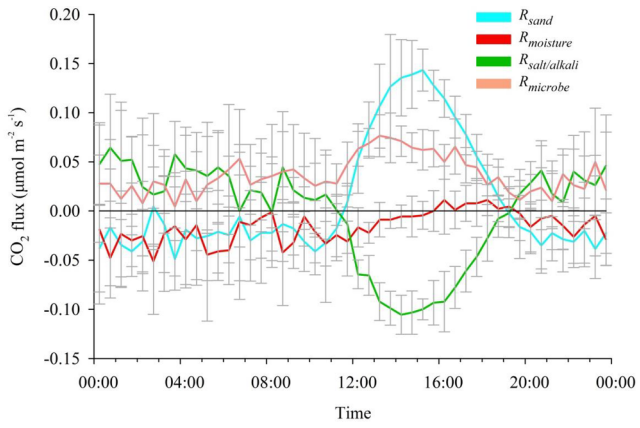

Fig. 3. The contribution of different components of shifting sand to the diurnal dynamic of the soil respiration of the Taklimakan Desert (TD) shifting sand was disassembled. The diurnal contributions of the CO_2 flux of each shifting sand component is expressed as R_{sand}, $R_{moisture}$, $R_{salt/alkali}$, and $R_{microbe}$, respectively. The error bars represent the standard deviation of the repeated CO_2 flux observations over many days.

established regression relationship between soil respiration, $T_{0–10cm}$, and $\Delta T_{10cm}/\Delta t$ cannot be directly applied. Using historical soil temperature data and monthly values of cumulative soil respiration obtained in the previous section, we re-established a relationship between cumulative monthly soil respiration and monthly average $T_{0–10cm}$. There was a good linear regression relationship between $T_{0–10cm}$ and the soil respiration of the TD shifting sand at the monthly scale:

$$R_s = 13641 \times T_{0-10cm} - 18814 \quad R^2 = 0.928 \tag{6}$$

where R_s (umol m^{-2} month^{-1}) is soil respiration at the monthly scale and $T_{0–10cm}$ is the soil temperature difference between 0 and 10 cm at the monthly scale. Finally, the total amount of soil respiration per year (i.e., carbon sink rate) in the TD shifting sand from 2018 to 2100 was obtained under the RCP4.5 and RCP8.5 scenarios.

3. Results

3.1. Contribution of each component to soil respiration

Compared to other ecosystems, soil respiration is significantly lower in shifting sand, which contains a superimposition of various components, with a negative CO_2 flux often present during the night (Lou and Zhou, 2006; Yang et al., 2017). The daily mean rate of soil respiration of shifting sand was 28.7 × 10^{-3} μmol·m^{-2}·s^{-1}, and the daily variation ranged from –0.026 to 0.101 μmol·m^{-2}·s^{-1}. In the disassembly experiment, we obtained the contribution of the CO_2 fluxes of various components in the TD shifting sand to the soil respiration, which is shown in Fig. 3. The contributions of sand and salts/alkalis were extremely significant, dominating the release and absorption of CO_2, respectively. For sand, the diurnal pattern of CO_2 flux followed a unimodal curve, with a higher intensity than in shifting sand. During the day, the sand promoted a CO_2 release into the atmosphere, which reached a peak (0.143 μmol·m^{-2}) at 15:15 h (Beijing time, used hereafter). During the night, sand promoted a stable CO_2 absorption from the atmosphere, with a mean rate of −0.026 μmol·m^{-2}. The contribution of moisture to soil respiration was very limited, with a rate ranging from −0.051 to 0.011 μmol·m^{-2}·s^{-1}. Moisture promoted the release of CO_2 to the atmosphere between 15:45 and 19:15 h and promoted atmospheric CO_2 absorption at other times. Because moisture had only a relatively small impact on the overall soil respiration, subsequent experiments focused on only the effects of soil temperature. During the day, salts/alkalis strongly absorbed atmospheric CO_2, reaching a peak (−0.106 μmol·m^{-2}) at 14:15 h whereas in the night, salts/alkalis promoted a stable CO_2 release into the atmosphere. Microbes were consistently responsible for a small amount of the CO_2 released into the atmosphere, and these effects were more pronounced during the day than the night.

3.2. Driving mechanisms of the CO_2 flux in sand

In the temperature-controlled experiments, sands without temperature regulation were relatively stable and temperature fluctuations in various layers during the entire observation period did not exceed 1 °C. The corresponding CO_2 flux was generally stable at approximately zero. By contrast, when the temperature was regulated there was a significant CO_2 absorption/release from the sand, the changing rhythm of which was generally consistent with variation in soil temperature (Fig. 4). As shown in the figure, the CO_2 flux increased when the soil temperature increased. When the soil temperature rapidly decreased, the CO_2 flux changed from initially positive to negative values. However, once soil temperatures became relatively stable, the CO_2 flux intensity began to exhibit a decreasing trend and gradually approached zero.

Based on the above information and considering that soil respiration indicates the overall performance of the soil surface layer (Lou and Zhou, 2006), we assert that the difference in soil temperature between depths of 0 and 10 cm ($T_{0–10cm}$) and the rate of change in soil temperature at a depth of 10 cm ($\Delta T_{10cm}/\Delta t$) are the two main factors driving the CO_2 flux in the sand (R_{sand}). The $T_{0–10cm}$ parameter represents the flow and intensity of soil heat, while $\Delta T_{10cm}/\Delta t$ represents heat absorption/release by the soil (Parsons et al., 2004; Ball et al., 2009). Compared to soil temperature, $T_{0–10cm}$ and $\Delta T_{10cm}/\Delta t$ were more consistent with R_{sand}, presenting significant linear and quadratic regression relationships, respectively (Fig. 5). This consistency could be enhanced, which was more evident after the soil temperature became stable. Besides, analyses of the synergistic effects showed that Eq. (4) could explain the comprehensive response of R_{sand} to the variation in $T_{0–10cm}$ and $\Delta T_{10cm}/\Delta t$ (Table 3). Through Eq. (4) and historical soil temperature data, the estimated values of R_{sand} were in good agreement with the observed values (Fig. 6).

3.3. Effect of $T_{0–10cm}$ and $\Delta T_{10cm}/\Delta t$ on R_s

Through the disassembly experiments, we found that soil temperature was the key factor controlling the contribution of the various components of soil respiration in the shifting sand. Therefore, we selected the soil respiration monitoring data for shifting sand in the study region and the corresponding soil temperatures of two layers (T_{0cm} and T_{10cm}) on January 17–31, 2013, October 17–23, 2013, May 4–7, 2015, and July 16–23, 2019, for analyses (Fig. 7). The $T_{0–10cm}$ and $\Delta T_{10cm}/\Delta t$ were consistent with R_s, with significant linear regression relationships (R^2 = 0.756 and 0.501, respectively; $P < 0.001$). Thus, we analyzed the synergistic effects of $T_{0–10cm}$ and $\Delta T_{10cm}/\Delta t$ on R_s (Table 3). Except for a failed fitting analysis when using Eq. (5), the other three equations explained the comprehensive responses of R_s to the variation in $T_{0–10cm}$ and $\Delta T_{10cm}/\Delta t$ ($R^2 > 0.756$) well and to a highly significant level ($P < 0.001$). This indicates that the synergistic effects of $T_{0–10cm}$ and $\Delta T_{10cm}/\Delta t$ were the major factors driving the CO_2 flux in the sand, and the main factors influencing soil respiration in shifting sand. In addition to the sand, other components also responded well to $T_{0–10cm}$ and $\Delta T_{10cm}/\Delta t$. Using Eq. (4) and corresponding observational data for soil temperature in different periods, the estimated values of R_s were in good agreement with the observed values (Fig. 8).

3.4. The response of the carbon sink rate of shifting sand to future climatic change

As shown in Fig. 9a, the mutual offset of the effects of thermal expansion of soil air containing CO_2 and the effects of the remaining

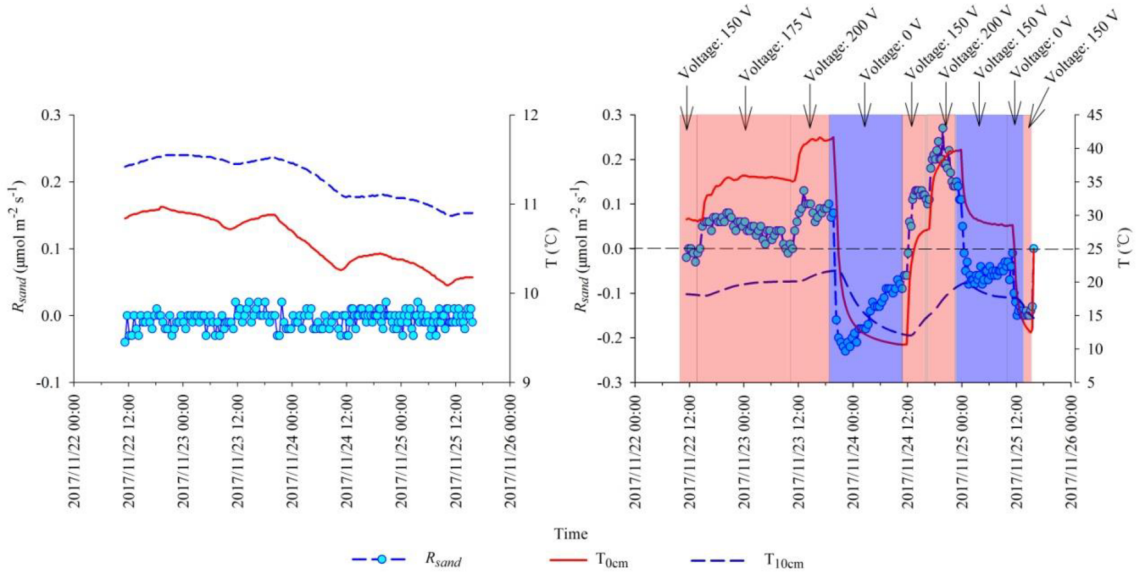

Fig. 4. Relationship between R_{sand} and soil temperatures at depths of 0 and 10 cm (T_{0cm} and T_{10cm}, respectively) in a temperature-controlled experiment using a voltage adjustment. Left: Unregulated soil temperature. Right: Regulated soil temperature. Black vertical lines separate regions of different voltages. Red regions correspond to voltage increases compared to the voltage in the preceding region, and subsequent increases in soil temperature. Blue regions correspond to voltage decreases compared to the voltage of the preceding region, and subsequent decreases in soil temperature. (For interpretation of the references to colour in this figure legend, the reader is referred to the web version of this article.)

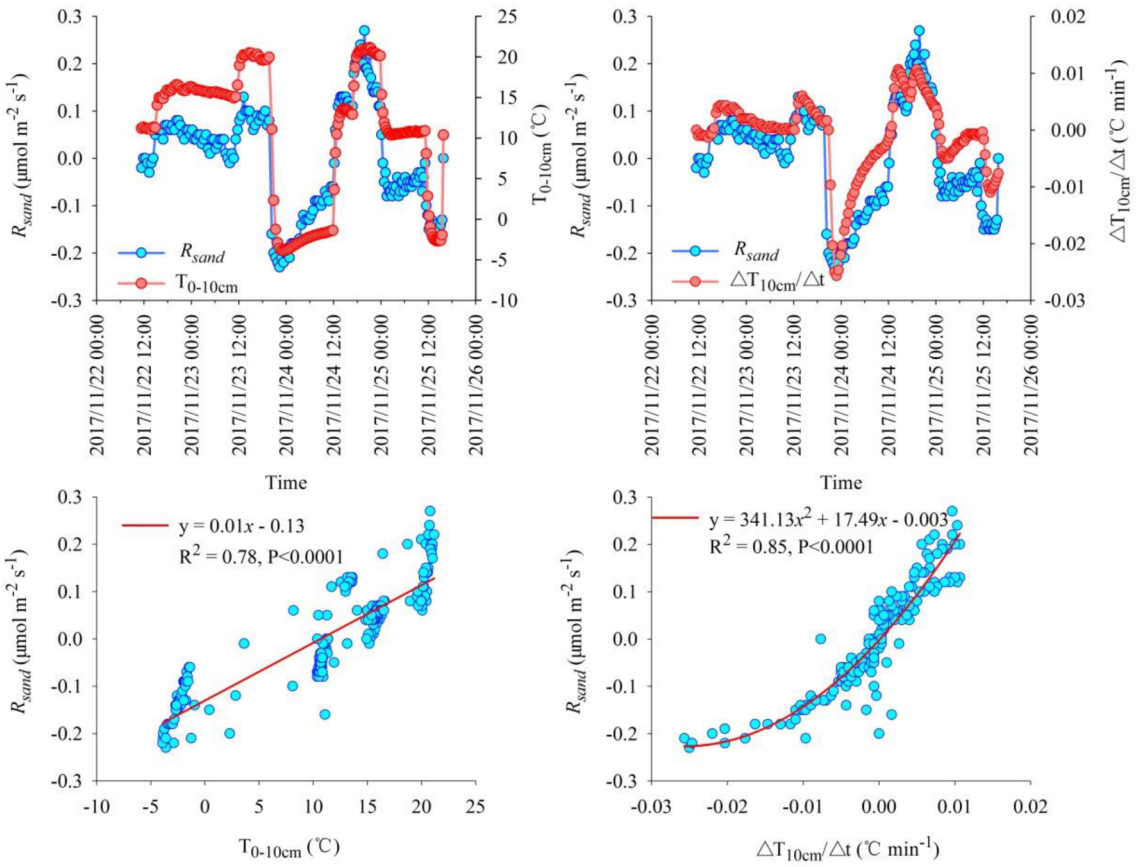

Fig. 5. Relationships between $T_{0–10cm}$, $\Delta T_{10cm}/\Delta t$, and R_{sand} in temperature-controlled experiments. Left: relationship between R_{sand} and $T_{0–10cm}$; Right: relationship between R_{sand} and $\Delta T_{10cm}/\Delta t$.

components (salt/alkali + moisture + microbes) caused the TD shifting sand to exhibit a clear and stable carbon sink effect, with an annual average CO_2 uptake rate of 7.11 g m^{-2} a^{-1}. Between 2004 and 2017, both processes increased over time. However, the increase in the rate of CO_2 released was higher than that of the CO_2 absorbed, which eventually caused an annually weakening trend in the carbon sink rate of shifting sand in TD. According to the relationship between $T_{0–10cm}$ and the carbon sink rate of the TD shifting sand, an increasing $T_{0–10cm}$

Table 3
Synergistic effect analysis for R_{sand}/R_s with $T_{0–10cm}$ and $\Delta T_{10cm}/\Delta t$.

	No.	Fitted equation	R^2
R_{sand}	2	$R_{sand} = 0.007 + 0.002\ T_{0–10cm} + 2.958\ \Delta T_{10cm}/\Delta t$	0.496**
	3	$R_{sand} = -0.010 + 0.002\ T_{0–10cm} + 1.542\ \Delta T_{10cm}/\Delta t + 0.108\ T_{0–10cm}\ \Delta T_{10cm}/\Delta t$	0.614**
	4	$R_{sand} = -0.031 - 0.002\ T_{0–10cm} + 4.116\ \Delta T_{10cm}/\Delta t + 0.0004\ T_{0–10cm}^{\ 2} - 67.961\ (\Delta T_{10cm}/\Delta t)^{\ 2}$	0.748**
	5	Failed	/
R_s	2	$R_s = -1.55 \times 10^{-4} + 0.008\ T_{0–10cm} - 2.445\ \Delta T_{10cm}/\Delta t$	0.756**
	3	$R_s = 0.007 + 0.008\ T_{0–10cm} - 2.147\ \Delta T_{10cm}/\Delta t - 0.048\ T_{0\text{-}10cm}\ \Delta T_{10cm}/\Delta t$	0.768**
	4	$R_s = -0.004 + 0.006\ T_{0–10cm} - 0.194\ \Delta T_{10cm}/\Delta t + 3.669 \times 10^{-5}\ T_{0–10cm}^{\ 2} - 35.928\ (\Delta T_{10cm}/\Delta t)^{\ 2}$	0.792**
	5	Failed	/

Notes: R^2 is the goodness-of-fit of the regression equation; '*' and '**' indicate a significant correlation at $P < 0.05$ and $P < 0.01$ (two-tailed), respectively. For R_{sand}, data from temperature-controlled experiments and field observations were combined to conduct the fitting analysis. For R_s, data from field observations were conducted the fitting analysis.

(Fig. 9c) in the future will more strongly stimulate the thermal expansion of soil air, pumping more CO_2 into the atmosphere, which will eventually lead to the gradual weakening of the carbon sink rate of the TD shifting sand. As shown in Fig. 9b, the carbon sink rate of the TD shifting sand will decrease at a rate of 0.43% and 1.20% per year under RCP4.5 and RCP8.5, respectively. The shifting sand surface in the TD was projected to reach a CO_2 absorption/release neutral state in approximately 2100 under RCP8.5. The weakening of the carbon sink rate was more pronounced under the RCP8.5 scenario.

4. Discussion

Based on the disassembly experiment, we obtained the contribution of the CO_2 fluxes of various components in the TD shifting sand to the soil respiration. To the best of knowledge, it is the firstever time to document the unconventional phenomenon that sand promoted a stable CO_2 exchange on the studies of soil respiration over the TD region. Due to the lack of a satisfactory explanation for this stimulating effect of sand at present, we designed subsequent temperature-controlled experiments and provided explanations for the mechanisms of affecting the diurnal pattern of sand CO_2 flux. Through observation experiments, we speculate that the expansion/contraction of soil air containing CO_2 by heat transmission caused sand to experience a CO_2 release/absorption phenomenon, which made an unexpected contribution to soil respiration. The intense increase/decrease in soil temperature promoted the expansion/contraction of soil air and resulted in the intense release/absorption of CO_2. Also, the loose and porous structure of sand allows the expansion/contraction of soil air during intense changes in temperature. Therefore, the soil temperature is the most critical driver of the CO_2 flux in the sand (Fang and Moncrieff, 2001; Sánchez et al., 2003; Rodeghiero and Cescatti, 2005). At the same time, the flow of soil heat in shifting sand makes the evaporation of deep soil water to present the diurnal variation. During daytime, the evaporation of deep soil water increased, and water vapor escaped from the surface, which increased the moisture content of extremely dry topsoil of shifting sand. This promoted the dissolution of soil carbonates and the absorption of atmospheric CO_2 by salt/alkali. In contrast, the carbonate reprecipitation in the nighttime promotes the release of CO_2 by salt/alkali (Walvoord et al., 2005; Schlesinger, 2017) which eventually leads to salt/alkali levels that strongly promots the absorption of atmospheric CO_2 in shifting sand during the day and release at night. The combined effects of this process and the expansion/contraction of soil air dominated the absorption/release of CO_2 in shifting sand. However, the minor fluctuations in soil moisture over the extremely dry TD area are not sufficient to overcome the limiting effects of drought on soil respiration, resulting in moisture making an extremely minor contribution to soil respiration in shifting sand. The above scenario has led to a new understanding of the role of moisture in the desert carbon cycle. The weak contribution of microbes to soil respiration indicated that microbial activity in the TD is very weak indicated that there are signs

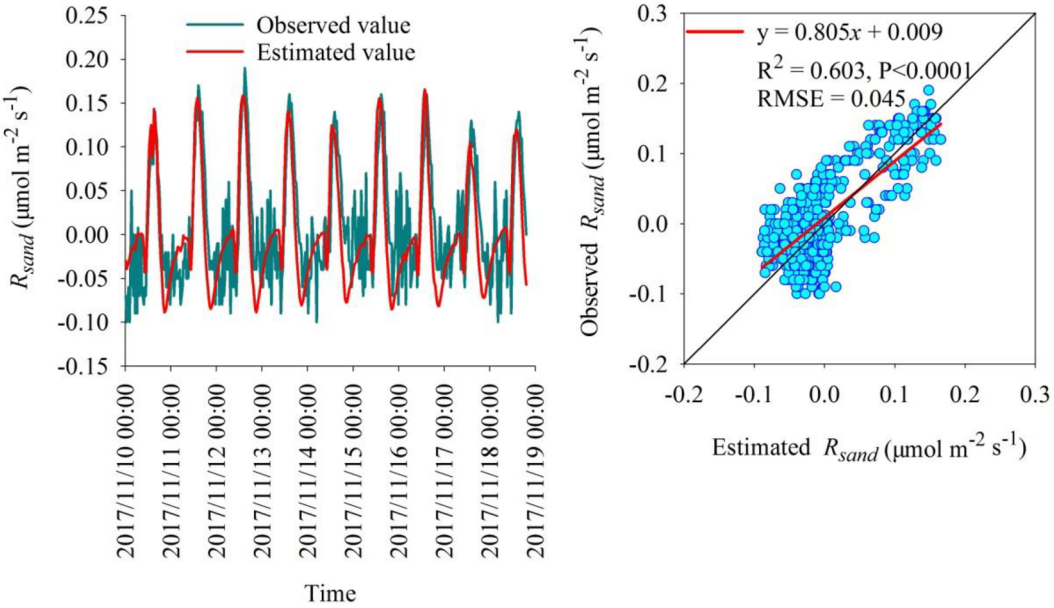

Fig. 6. Comparison of R_{sand} obtained from experimental data and estimated by equation (4) in sand. Left: Time series of observed and estimated R_{sand}. Right: Regression relationship between observed and estimated R_{sand}.

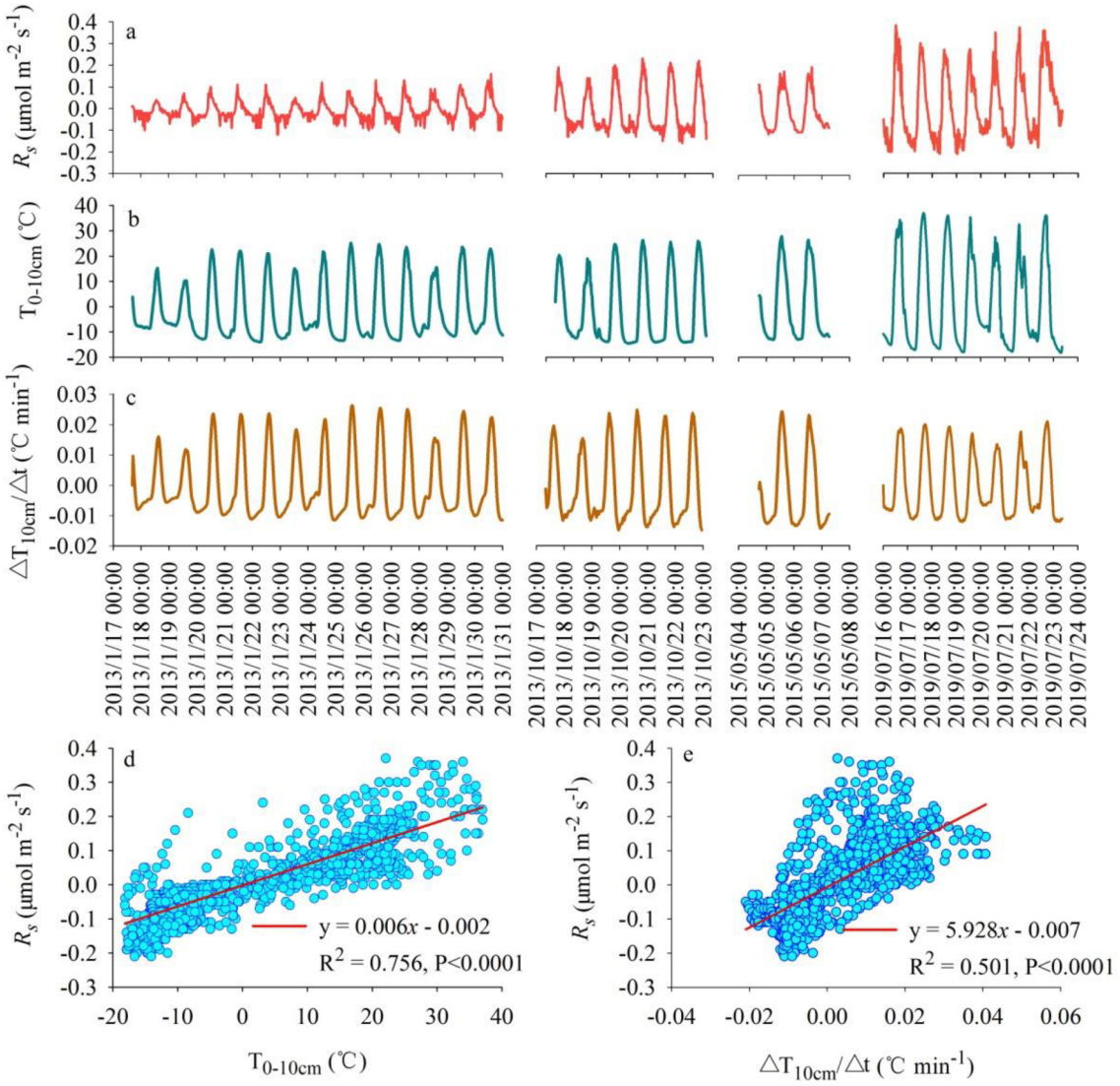

Fig. 7. Relationships among $T_{0–10cm}$, $\Delta T_{10cm}/\Delta t$, and R_s during January 17–31, 2013, October 17–23, 2013, May 4–7, 2015, and July 16–23, 2019. a–c, Time series of (a) R_s, (b) $T_{0–10cm}$, and (c) $\Delta T_{10cm}/\Delta t$. d, Regression analyses between R_s and $T_{0–10cm}$. e, Regression analyses between R_s and $\Delta T_{10cm}/\Delta t$.

of life in the desert, which is not as lifeless as it appeared.

The superimposition of several processes caused TD shifting sand to exhibit an incredible carbon sink effect, with an annual average CO_2 uptake rate of 7.11 g m^{-2}·a^{-1} during 2004–2017. This may account for part of the missing carbon sink in the global carbon cycle. Global warming will accelerate the decomposition of organic carbon, releasing large amounts of CO_2 into the atmosphere (Bond-Lamberty and Thomson, 2010; Giardina et al., 2014). However, in desert ecosystems, with extremely low organic carbon reserves, increases in $T_{0–10cm}$ due to climate change will strongly stimulate the future thermal expansion of soil air, releasing more CO_2 from the sand into the atmosphere. This process will eventually lead to a gradual weakening of the carbon sink rate in the TD shifting sand. Under RCP4.5 and RCP8.5, the CO_2 uptake rate in the TD shifting sand will decrease by 0.43% and 1.20% per year, respectively. Under RCP8.5, the shifting sand surface in the TD was projected to reach a CO_2 absorption/release neutral state in approximately 2100. This would facilitate a positive feedback effect under climate change, causing enhanced warming in an arid and semi-arid area, and may have profound effects on the societal welfare (Rustad et al., 2000; Friedlingstein et al., 2001; Huang et al., 2008, Huang et al., 2016, Huang et al., 2018). Desert ecosystems, which have long been undervalued, have always played in obscurity an important role as carbon sinks. However, a gradual reduction in the ability of deserts to act as carbon sinks will put forward more urgent requirements for the formulation of climate change countermeasures.

5. Conclusions

Based on dismantling and temperature-controlled experiments, our study quantified the exact magnitude and process of the CO_2 fluxes for each component of the shifting sand in the TD. In particular, it considered the process of soil air expansion/contraction, which is easily neglected, and the exaggerated effect of soil moisture on the CO_2 flux in a desert environment. Furthermore, the absorption of CO_2 by saline/alkali factors in the desert was confirmed. Finally, we found that the TD shifting sand currently acts as a stable carbon sink that had an annual CO_2 uptake rate of 7.11 g m^{-2}·a^{-1} during 2004–2017. If all global shifting deserts are considered, the status of desert ecosystems in the global carbon cycle cannot be ignored. These results could help to account for part of the missing carbon sink in the global carbon cycle. However, CMIP5 simulations indicate that the contribution of the TD shifting sand carbon sink will decrease in the future through over-stimulation of the unnoticed temperature-driven process of soil air expansion in the CO_2 release process.

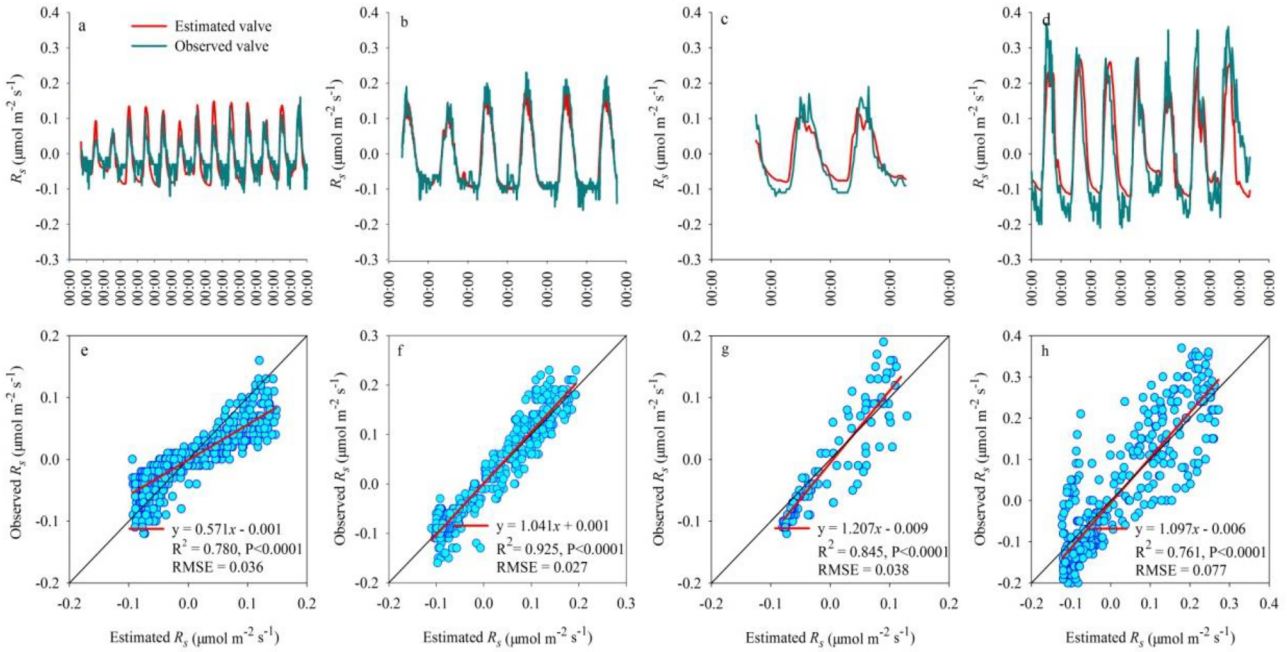

Fig. 8. Comparison of R_s obtained from experiments and estimated by equation (4) in shifting sand. a-d, Relationships between the observed and estimated R_s are shown for (a) January 17–31, 2013, (b) October 17–23, 2013, (c) May 4–7, 2015, and (d) July 16–23, 2019 and. e-h, The regression relationships for the time periods are shown in (a–d).

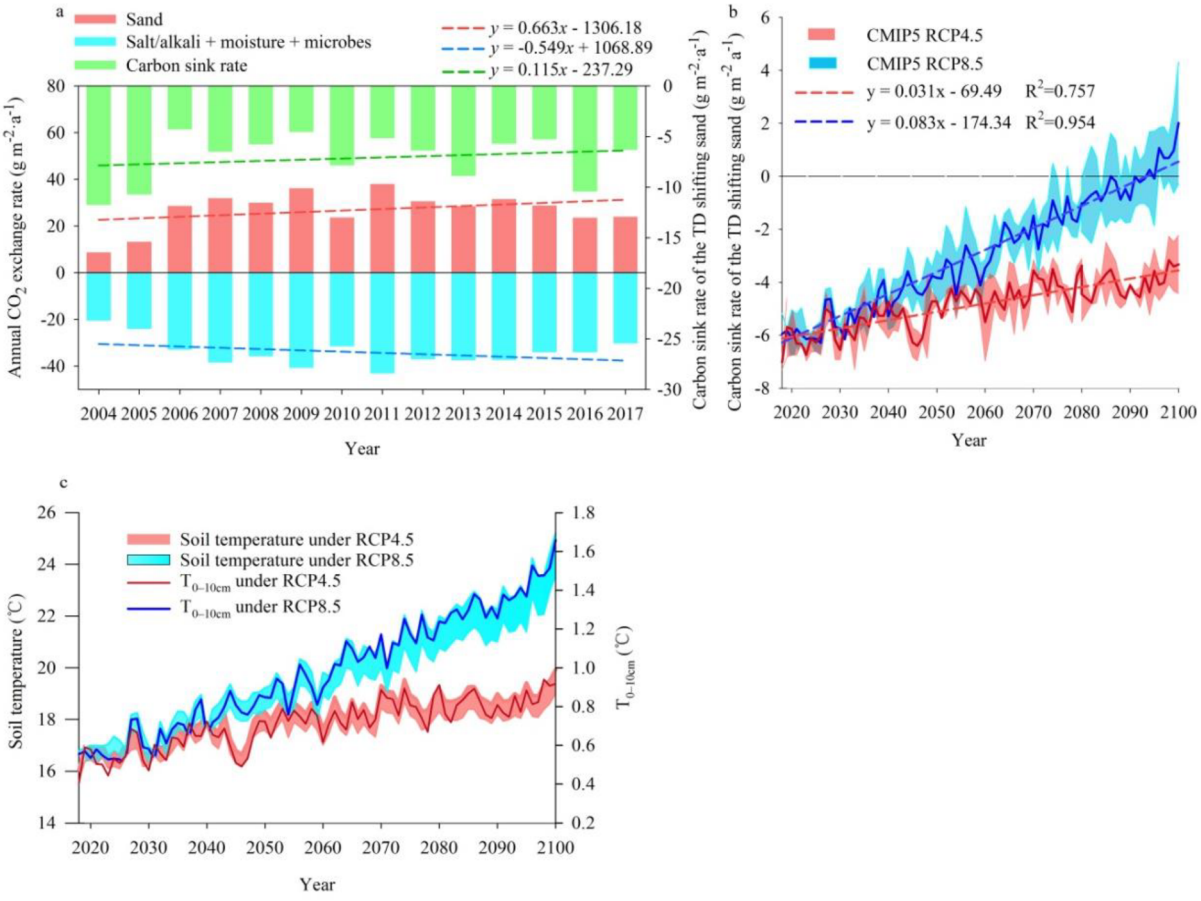

Fig. 9. Temporal variation of annual CO_2 exchange rate of shifting sand in the Taklimakan Desert (TD). a, Temporal variation in the soil CO_2 exchange rate per year for 2004–2017 in TD shifting sand. b, Under Representative Concentration Pathway (RCP) scenarios 4.5 and 8.5, temporal variation in the carbon sink rate for 2018–2100 in TD shifting sand. Shading denotes the mean ± standard deviation of three models (MIROC5, MRI-CGCM3, and CMCC-CMS). c, Temporal variation in soil temperature and $T_{0–10cm}$ under the RCP scenarios 4.5 and 8.5. The upper boundary of the shading denotes the soil temperature at 0 cm, and the lower boundary denotes the soil temperature at 10 cm.

Declaration of Competing Interest

The authors declare that they have no known competing financial interests or personal relationships that could have appeared to influence the work reported in this paper.

Acknowledgments

This work was jointly supported by the second Tibetan Plateau Scientific Expedition and Research Program [grant number 2019QZKK0602], the National Natural Science Foundation of China [grant numbers 41521004, 41975010 and 41175140], the China University Research Talents Recruitment Program [111 Project; grant number B13045] and the Tianshan Youth Talents Plan Project of Xinjiang [Fan Yang].

Appendix A. Supplementary data

Supplementary data to this article can be found online at https://doi.org/10.1016/j.geoderma.2020.114636.

References

Ball, B.A., Virginia, R.A., Barrett, J.E., Parsons, A.N., Wall, D.H., 2009. Interactions between physical and biotic factors influence CO_2 flux in Antarctic dry valley soils. Soil Biol. Biochem. 41, 1510–1517.

Bond-Lamberty, B., Thomson, A., 2010. Temperature-associated increases in the global soil respiration record. Nature 464, 579–582.

Bond-Lamberty, B., 2018. New techniques and data for understanding the global soil respiration flux. Earths Future 6, 1176–1180.

Chen, X., Wang, W.F., Luo, G.P., Ye, H., 2014. Can soil respiration estimate neglect the contribution of abiotic exchange? J. Arid Land 6, 129–135.

Cuezva, S., Fernandez-Cortes, A., Benavente, D., Serrano-Ortiz, P., Kowalski, A.S., Sanchez-Moral, S., 2011. Short-term CO_2(g) exchange between a shallow karstic cavity and the external atmosphere during summer: Role of the surface soil layer. Atmos. Environ. 45, 1418–1427.

Fa, K.Y., Liu, J.B., Zhang, Y.Q., Wu, B., Qin, S.G., Feng, W., Lai, Z.R., 2014. CO_2 absorption of sandy soil induced by rainfall pulses in a desert ecosystem. Hydrol. Process. 29, 2043–2051.

Fa, K.Y., Zhang, Y.Q., Wu, B., Qin, S.G., Liu, Z., She, W.W., 2016. Patterns and possible mechanisms of soil CO_2 uptake in sandy soil. Sci. Total Environ. 544, 587–594.

Fang, C., Moncrieff, J.B., 2001. The dependence of soil CO_2 efflux on temperature. Soil Biol. Biochem. 33, 155–165.

Friedlingstein, P., Bopp, L., Ciais, P., Dufresne, J.L., Fairhead, L., LeTreut, H., Monfray, P., Orr, J., 2001. Positive feedback between future climate change and the carbon cycle. Geophys. Res. Lett. 28, 1543–1546.

Giardina, C.P., Litton, C.M., Crow, S.E., Asner, G.P., 2014. Warming-related increases in soil CO_2 efflux are explained by increased below-ground carbon flux. Nat. Clim. Change 4, 822–827.

Gu, F.X., Wen, Q.K., Pan, B.R., Yang, Y.S., 2000. A preliminary study on soil micoorganisms of artificial vegetation in the center of Taklimakan Desert. Chin. Biodivers. 8, 297–303 (in Chinese).

Hamerlynck, E.P., Scott, R.L., Sánchez-Cañete, E.P., Barron-Gafford, G.A., 2013. Nocturnal soil CO_2 uptake and its relationship to subsurface soil and ecosystem carbon fluxes in a Chihuahuan Desert shrubland. J. Geophys. Res-Biogeo. 118, 1593–1603.

Han, Q.F., Luo, G.P., Li, C.F., Li, S.B., 2018. Response of carbon dynamics to climate change varied among different vegetation types in Central Asia. Sustainability 10, 3288. https://doi.org/10.3390/su 10093288.

Hashimoto, S., Carvalhais, N., Ito, A., Migliavacca, M., Nishina, K., Reichstein, M., 2015. Global spatiotemporal distribution of soil respiration modeled using a global database. Biogeosciences 12, 4121–4132.

Houghton, R.A., Davidson, E.A., Woodwell, G.M., 1998. Missing sinks, feedbacks, and understanding the role of terrestrial ecosystems in the global carbon balance. Global Biogeochem. Cy. 12, 25–34.

Huang, J.P., Zhang, W., Zuo, J.Q., Bi, J.R., Shi, J.S., Wang, X., Chang, Z.L., Huang, Z.W., Yang, S., Zhang, B.D., Wang, G.Y., Feng, G.H., Yuan, J.Y., Zhang, L., Zuo, H.C., Wang, S.G., Fu, C.B., Chou, J.F., 2008. An overview of the semi-arid climate and environment research observatory over the Loess Plateau. Adv. Atmos. Sci. 25, 906–921.

Huang, J.P., Yu, H.P., Guan, X.D., Wang, G.Y., Guo, R.X., 2016. Accelerated dryland expansion under climate change. Nat. Clim. Change 6, 166–171.

Huang, J.P., Huang, J.P., Liu, X.Y., Li, C.Y., Ding, L., Yu, H.P., 2018. The global oxygen budget and its future projection. Sci. Bull. 63, 1180–1186.

Huo, W., He, Q., Yang, X.H., Liu, X.C., Ding, G.F., Cheng, Y.J., 2011. The research on grain size characteristic of desert in north of China. Res. Soil Water Conserv. 18, 6–11 (in Chinese).

Jian, J., Steele, M.K., Thomas, R.Q., Day, S.D., Hodges, S.C., 2018. Constraining estimates of global soil respiration by quantifying sources of variability. Global Change Biol. 24, 4143–4159.

Li, C.F., Han, Q.F., Luo, G.P., Zhao, C.Y., Li, S.B., Wang, Y.G., Yu, D.S., 2018. Effects of cropland conversion and climate change on agrosystem carbon balance of China's dryland: A typical watershed study. Sustainability 10, 4508. https://doi.org/10.3390/su 10124508.

Li, Y., Wang, Y.G., Houghton, R.A., Tang, L.S., 2015. Hidden carbon sink beneath desert. Geophys. Res. Lett. 42, 5880–5887.

Lou, Y.Q., Zhou, X.H., 2006. Soil Respiration and the Environment. San Diego. Academic Press/Elsevier, pp. 1–89.

Ma, J., Wang, Z.Y., Stevenson, B.A., Zheng, X.J., Li, Y., 2013. An inorganic CO_2 diffusion and dissolution process explains negative CO_2 fluxes in saline/alkaline soils. Sci. Rep. 3. https://doi.org/10.1038/srep02025.

Ma, J., Liu, R., Tang, L.S., Lan, Z.D., Li, Y., 2014. A downward CO_2 flux seems to have nowhere to go. Biogeosciences 11, 6251–6262.

Parsons, A.N., Barrett, J.E., Wall, D.H., Virginia, R.A., 2004. Soil carbon dioxide flux in Antarctic dry valley ecosystems. Ecosystems 7, 286–295.

Rodeghiero, M., Cescatti, A., 2005. Main determinants of forest soil respiration along an elevation/temperature gradient in the Italian Alps. Global Change Biol. 11, 1024–1041.

Rustad, L.E., Huntington, T.G., Boone, R.D., 2000. Controls on soil respiration: Implications for climate change. Biogeochemistry 48, 1–6.

Sánchez, M.L., Ozores, M.I., López, M.J., Colle, R., Torre, B.D, García, M.A., Pérez, I., 2003. Soil CO2 fluxes beneath barley on the central Spanish plateau. Agr. Forest Meteorol. 118, 85-95.

Schlesinger, W.H., Andrews, J.A., 2000. Soil respiration and the global carbon cycle. Biogeochemistry 48, 7–20.

Schlesinger, W.H., 2017. An evaluation of abiotic carbon sinks in deserts. Global Change Biol. 23, 25–27.

Shanhun, F.L., Almond, P.C., Clough, T.J., Smith, C.M.S., 2012. Abiotic processes dominate CO_2 fluxes in Antarctic soils. Soil Biol. Biochem. 53, 99–111.

Singh, J.S., Gupta, S.R., 1977. Plant decomposition and soil respiration in terrestrial ecosystems. Bot. Rev. 43, 449–528.

Stone, R., 2008. Have desert researchers discovered a hidden loop in the carbon cycle? Science 320, 1409–1410.

Wang, Y.M., Wang, J.H., Yan, C.Z., 2005. Data set of desert (sand) distribution in China with scale of 1:100000. Cold Arid Regions Sci. Data Center Lanzhou. https://doi.org/10.3972/westdc.006.2013.db.

Wang, Z.Y., Xie, J.B., Wang, Y.G., Li, Y., 2013. Soil inorganic CO_2 flux in relation to soil pH and electric conductivity in saline/alkaline soils. Chin. J. Ecol. 32, 2552–2558 (in Chinese).

Walvoord, M.A., Strieg, R.G., Prudic, D.E., Stonestrom, D.A., 2005. CO_2 dynamics in the Amargosa Desert: Fluxes and isotopic speciation in a deep unsaturated zone. Water Resour. Res. 41, W02006.

Xie, J.X., Li, Y., Zhai, C.X., Li, C.H., Lan, Z.D., 2009. CO_2 absorption by alkaline soils and its implication to the global carbon cycle. Environ. Geol. 56, 953–961.

Xu, M., Shang, H., 2016. Contribution of soil respiration to the global carbon equation. J. Plant Physiol. 203, 16–28.

Yang, F., Ali, M., Zheng, X.Q., He, Q., Yang, X.H., Huo, W., Liang, F.C., Wang, S.M., 2017. Diurnal dynamics of soil respiration and the influencing factors for three land-cover types in the hinterland of the Taklimakan Desert China. J. Arid Land 9, 568–579.

Yang, X.H., Yang, F., Liu, X.C., Huo, W., Ali, M., Zhang, Q.Y., 2016a. Comparison of horizontal dust fluxes simulated with two dust emission schemes based on field experiments in Xinjiang China. Theor. Appl. Climatol. 126, 223–231.

Yang, X.H., Shen, S.H., Yang, F., He, Q., Ali, M., Huo, W., Liu, X.C., 2016b. Spatial and temporal variations of blowing dust events in the Taklimakan Desert. Theor. Appl. Climatol. 125, 669–677.

Zhou, C.L., Ali, M., Yang, F., Huo, W., Wang, M.Z., Pan, H.L., He, Q., Jin, L.L., Yang, X.H., 2019. Dust uplift potential in the Taklimakan Desert: An analysis based on different wind speed measurement intervals. Theor. Appl. Climatol. 137, 1449–1456.